CHINESE OPTICS LETTERS

Vol. 21, No. 5 | May 2023

Highly efficient, tunable, ultrabroadband NIR photoemission from Bi-doped nitridated germanate glasses toward all-band amplification in optical communication

Fuguang Chen (陈福广)[1], Zhi Chen (陈 智)[1*], Jianrong Qiu (邱建荣)[2], Shuai Zhang (张 帅)[3**], and Zhijun Ma (马志军)[1***]

[1] Research Center for Humanoid Sensing, Zhejiang Lab, Hangzhou 311121, China

[2] State Key Laboratory of Modern Optical Instrumentation, College of Optical Science and Engineering, Zhejiang University, Hangzhou 310027, China

[3] Zhejiang Chinese Medical University, Hangzhou 311100, China

*Corresponding author: zhichen@zhejianglab.edu.cn

**Corresponding author: zhsrenl@163.com

***Corresponding author: zhijma@zhejianglab.com

Received November 16, 2022 | Accepted January 17, 2023 | Posted Online May 11, 2023

Bismuth (Bi)-doped near-infared (NIR) glass that can cover the entire optical communication window (850, 1310, and 1550 nm) has become the subject of extensive research for developing photonic devices, particularly, tunable fiber lasers and ultrabroadband optical amplifiers. However, the realization of highly efficient NIR luminescence from Bi-doped glass is still full of challenges. Notably, due to the co-existence of multiple Bi NIR centers in the glass, the origin of newly generated Bi NIR emission peaks at ~930 and ~1520 nm is still controversial. Here, we report a new Bi-doped nitridated germanate glass with tunable ultrabroadband NIR emission (850–1700 nm) and high external quantum efficiency (EQE) of ~50%. A series of studies, including spectral analysis, nuclear magnetic resonance (NMR), and others, provide powerful evidence for the mechanism of luminescence enhancement and tunability, and make reasonable inferences about the origin of the new emission bands at ~930 and ~1520 nm. We believe that the results discussed above would enrich our understanding about multiple Bi NIR emission behaviors and contribute to the design and fabrication of highly efficient Bi-doped ultrabroadband wavelength-tunable optical glass fiber amplifiers and lasers in the future.

Keywords: bismuth; germanate glass; near-infrared luminescence.

DOI: 10.3788/COL202321.051601

1. Introduction

With the arrival of a new era of cloud storage, the Internet of things, and 5G/6G, the demand for improving information transmission capacity in optical communication systems, which is limited by the gain spectra of fiber amplifiers, is even more urgent[1–3]. To satisfy this need, novel photonic materials with highly efficient and ultrabroadband near-infrared (NIR) emission performance have been pursued for a long time. Traditionally, rare earth (RE)- or transition metal (TM)-doped glasses, glass ceramics, or glass fibers can exhibit higher NIR emission efficiency; however, the narrow gain bandwidth (not exceeding 100 nm) of RE ions[4–6] and the requirement of suitable crystal field for TM ion-doped glass[7,8], have resulted in limited success.

Alternatively, Bi-doped glasses and fibers, found by Y. Fujimoto in 1999[9,10], presenting ultrabroadband NIR luminescence features from 1000 to 1600 nm, have drawn extensive attention, which enables ultrabroadband gain material for full-wavelength amplification covering the entire optical communication window[11–14]. However, the insufficient efficiency and low gain are the critical defects limiting the application of Bi-based fiber. Therefore, how to improve the NIR luminescence performance of Bi-doped glasses is of great importance to promote the development of the Bi-doped fibers toward highly efficient optical amplifiers and tunable lasers. Over the past two decades, various strategies have been attempted, ranging from modulating the glass networks, optimizing the melting regime (such as melting or annealing temperature, time, and

atmosphere), using high-energy radiation or crystallization, co-doping other active NIR centers, to improving the NIR emission intensity and bandwidth of Bi-doped glasses.

To enhance the NIR emission intensity by modulating the glass networks will result in worse thermal properties of Bi-doped glasses (such as soft point and refractive index) at the same time, which will make it complicated to prepare the desired fibers[15–18]. For optimizing the melting regime, it usually generates little effect when adjusting the melting or annealing temperature and time[19,20]. However, melting in the H_2 atmosphere will greatly enhance the emission intensity of Bi-doped glasses, but it is difficult and dangerous to control the reduction progress due to the rapid reaction at high temperatures[21]. The use of high-energy radiation or crystallization to enhance the NIR emission intensity of Bi-doped glasses both bring challenges to fabricating fibers[22,23]. Moreover, co-doping rare earth (RE) or TM active centers is a simple and commonly used method to broaden the NIR emission range to cover the whole optical communication window, but it is also faced with the problem of requiring coupling of multiple pump sources[24,25]. Hence, it remains challenging to intensify and broaden Bi NIR emission in a proper way.

In this work, we developed a new Bi-doped nitridated germanate glass with tunable ultrabroadband photoemission (850–1700 nm), an enhancement of ~70 times for the integrated intensity of Bi-related four emission bands, and a high external quantum efficiency (EQE) of ~50% by regulating the short-to medium-range order of the glass via manipulation of Al_2O_3, as sketched in Fig. 1. To elucidate how the multiple Bi NIR centers respond to variations of Al_2O_3 introduced into the glass matrices, a series of microstructure analyses, including Fourier-transform infrared (FTIR) spectroscopy, Raman spectroscopy, ^{27}Al nuclear magnetic resonance (NMR), have been leveraged. Here, the results show that the conversion among AlO_6, AlO_5, and AlO_4 leads to the enhancement and different behaviors of Bi NIR emission. Nevertheless, introducing excessive Al_2O_3 into the glass will contribute to formation of local excess negative charges, resulting in low-valence Bi being oxidized into high-valence. Thus, a Bi-doped nitridated germanate glass with highly efficient, tunable, and ultrabroadband NIR luminescence, covering the entire optical communication window, can be achieved by reasonable design and manipulation of Al_2O_3. We believe that this work will contribute to the design and fabrication of Bi-doped glass fiber with highly efficient, tunable, and ultrabroadband NIR emission and provide deep insight into the mechanism of the multiple Bi NIR centers.

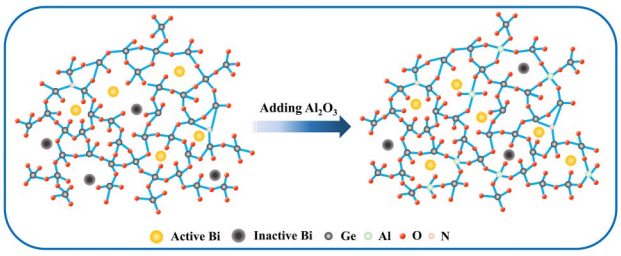

Fig. 1. Evolution of the microscopic structure of Bi-doped nitridated germanate glass with the introduction of Al_2O_3.

2. Experimental Setup

2.1. Sample synthesis

Glass samples with molar composition of $(87-x)GeO_2$-xAl_2O_3-10BaO-3AlN-0.02 Bi_2O_3 ($x = 0, 3, 6, 8, 9, 10, 11, 12, 13$), where x denotes the content of Al_2O_3 in the glass sample, were prepared by the melting and quenching method. Analytical grade Al_2O_3, $BaCO_3$, and high-purity GeO_2, AlN, and Bi_2O_3 (99.99%) were used as starting materials. Batches of raw materials weighting 20 g were mixed homogeneously in an agate mortar. Each batch of the mixture was melted in an alumina crucible at a temperature of 1520°C in air for 30 min. Before the glass was formed, a quartz glass rod was used to stir the glass liquid evenly to achieve uniform mixing to a certain degree. Afterwards, the melt was cast onto a stainless-steel plate and pressed by another stainless-steel plate simultaneously so as to speed up the cooling process and avoid crystallization, and eventually form solid-state glass (labeled as xAl, according to the values of x). Finally, the glasses were cut and polished for subsequent optical analysis.

2.2. Characterization

Optical absorption spectra of the samples were measured by using a Perkin Elmer Lambda 900 UV/VIS spectrophotometer covering the spectral range of 300–1200 nm. Static excitation and emission spectra, dynamic emission spectra excited at 460 nm, and luminescence lifetime were recorded by using an Edinburgh FLS920 spectrofluorometer equipped with a continuous-wave 450 W Xe lamp and a microsecond flashlamp (μF900) as excitation sources, respectively. The EQE of the samples was measured by an absolute photoluminescence (PL) quantum yield spectrometer (Quantaurus-QY Plus C13534-11, Hamamatsu Photonics). X-ray diffraction (XRD) patterns were characterized by using an X-ray diffractometer (Rigaku D/max-IIIA) with Cu Kα1 radiation (1.5405 Å; cathode voltage, 40 kV; current, 40 mA) in the 2θ range of 10°–80°. FTIR profiles were measured in transmission mode with a Bruker Vector 33 spectrometer by dispersing glass powders into KBr pellets. Raman spectra were obtained via a Raman spectrometer (Renishaw inVia) excited by a Nd:YAG laser at 532 nm with a power of 25 mW. A Bruker AVANCE III HD 400 instrument equipped with high-speed magic angle spinning (MAS) probe heads was used to measure the ^{27}Al NMR spectra. If not being specially stated, all measurements were conducted at room temperature.

3. Experimental Results and Discussion

The NIR PL emission spectra of the glass samples containing different contents of Al_2O_3 over 0–13% (molar fraction), upon

460 nm excitation, are depicted in Fig. 2(a). It can clearly be observed that all the samples present ultrabroadband emission from 850 to 1700 nm and consist of four emission peaks located at ~930, ~1160, ~1260, and ~1520 nm, respectively. The emission peak at ~1160 nm originates mainly from the typical transition of $^3P_1 \rightarrow {}^3P_0$ from Bi^+, while the emission band at ~1260 nm is assigned to $^4S_{3/2} \rightarrow {}^2P_{1/2}$ of Bi^0[16,26–28], and the origin of newly generated Bi NIR emission centered at ~930 and ~1520 nm is still controversial[29,30], the nature of which will be explored and interpreted in the following. Moreover, the intensity of the ultrabroadband NIR emission can dramatically be enhanced (that is, the integrated intensity is enhanced by ~77 times for 11Al sample compared to that of 0Al sample) by regulating the content of Al_2O_3, and, the EQE of the glass without Al doping is only 2.52%, while that of 11Al is up to ~50% [Fig. 2(c)], which has never been reported in Bi-doped NIR glasses[31], and shows great potential for an ultrabroadband NIR light source. Interestingly, the relative intensity ($I_{1260\,nm}/I_{1160\,nm}$) of emission peaked at 1160 and 1260 nm can also be modulated by tuning the concentration of Al_2O_3, showing a monotonically decreasing trend with an increase of Al_2O_3 content, as plotted in Fig. 2(b) and Fig. S1 (see Supplementary Material for more information). Moreover, the emission intensities at ~930 and ~1520 nm share a similar decreasing trend with that of ~1260 nm, which provides important clues to exploring the origin of the newly generated emission bands at ~930 and ~1520 nm.

The UV–VIS–NIR absorption feature of Bi-doped nitridated germanate glass with various Al_2O_3 doping was examined. As presented in Fig. 3(a), the glass free of Al_2O_3 shows no visible

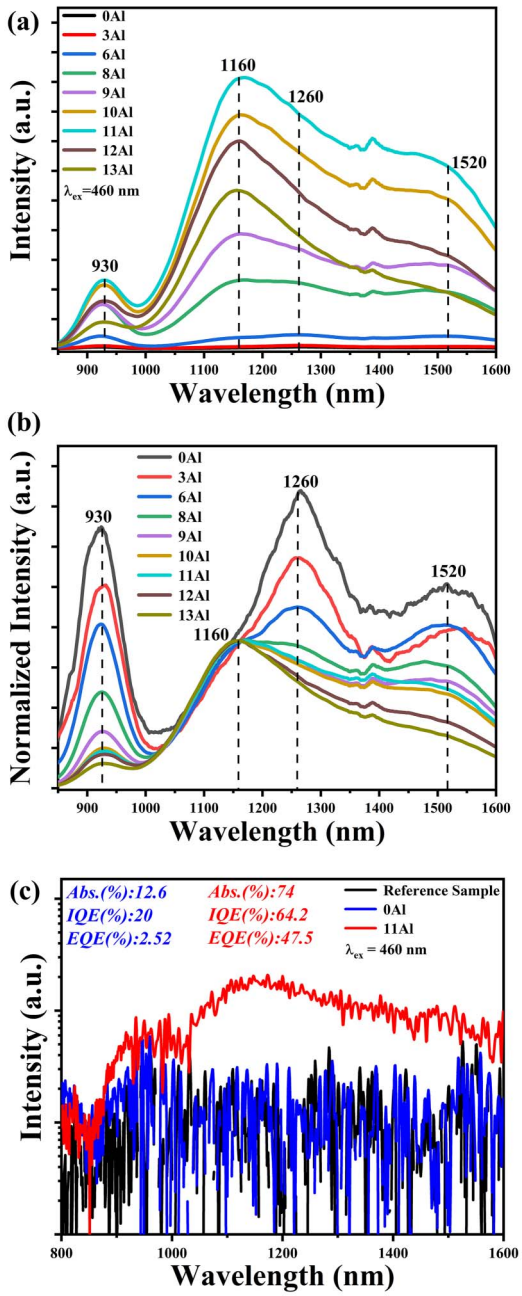

Fig. 2. (a) NIR PL emission spectra ($\lambda_{ex} = 460$ nm) of Bi-doped nitridated germanate glasses containing xAl_2O_3 (x = 0–13%); (b) corresponding emission spectra normalized to the emission peak at 1160 nm; (c) emission spectra inside the integrating sphere without and with the sample 0Al or 11Al upon 460 nm excitation; inset shows the magnified spectra in the wavelength range of 800 to 1600 nm.

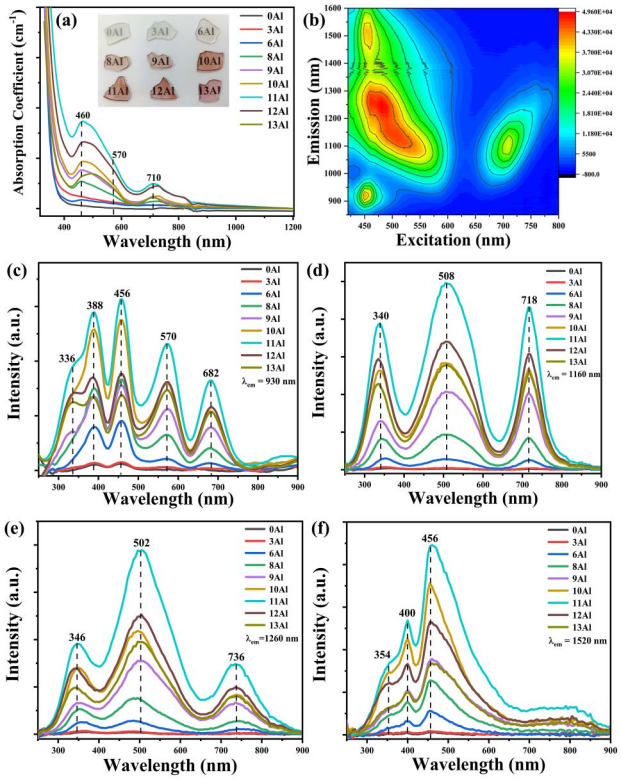

Fig. 3. (a) Optical absorption spectra of the glass samples containing xAl_2O_3 (x = 0–13%); (b) contour plot of the emission-excitation map from the 6Al glass sample; corresponding PL excitation spectra monitored at (c) 930 nm, (d) 1160 nm, (e) 1260 nm, and (f) 1520 nm of the glass samples containing xAl_2O_3 (x = 0–13%).

absorption, indicating that there are few activate NIR centers in the sample. Nevertheless, a small amount of alumina leads to fantastic changes of characteristic absorption of Bi NIR centers in the range of 300–1200 nm. By increasing the Al_2O_3, three obvious absorption peaks located at ~460, ~570, and ~710 nm appear, in accordance with the typical transition of $^4S_{3/2} \rightarrow {}^2P_{1/2}$ from Bi^0, newly generated Bi NIR center, and $^3P_0 \rightarrow {}^3P_2$ from Bi^+, respectively. Moreover, the absorption intensity increases further as Al_2O_3 varies from 0 to 11%, and reaches the optimum for the 11Al glass sample, but an opposite phenomenon occurs when further increasing Al_2O_3 content. The parallel variation between NIR PL and absorption spectra evidences that the number of multiple Bi NIR activation centers can be adjusted by controlling the Al_2O_3 concentration.

To reveal the deeper relationship between emission peaks and excitation wavelength in more detail, the dependence of emission peaks on excitation wavelength has been studied (Fig. S2; see Supplementary Material), and the contour plot of NIR emission-excitation map from 6Al glass sample was collected as shown in Fig. 3(b). Clearly, the Bi NIR centers show different responses when varying the excitation wavelength from 420 to 750 nm. When monitoring at ~1260 nm (Bi^0), a wide absorption band from 454 to 500 nm was observed. Similarly, the centers at ~930 and 1520 nm can only be excited at around 460 nm. This similar feature gives another clue that the root of the newly generated NIR centers at ~930 and 1520 nm may be related to ~1260 nm (Bi^0). The emission at ~1160 nm (Bi^+), however, can simultaneously be excited by blue light (480–520 nm) and red light (~700 nm). The result discussed above further confirms that at least three types of Bi NIR centers coexist in the germanate glass.

To obtain more clues on active Bi NIR centers, the excitation spectra of the four emission bands were collected. As shown in Figs. 3(c)–3(f), the active Bi NIR centers share diverse excitation dependent features, which is consistent with the above discussion. On one hand, all the observed active Bi NIR centers absorb UV–VIS light and can be well excited by blue light, which matches well with commercial blue LEDs and shows great potential for blue LED-excited ultrabroadband NIR light sources. In addition, all the excitation intensities reach the optimum state at $x = 11$, and decrease with further increasing Al_2O_3 content with respect to the absorption and emission spectra. On the other hand, the four excitation spectra are different in some details. The emission band at 1160 nm shares three excitation bands at ~340, ~508, and ~718 nm, respectively. However, the emission band at 1260 nm has two weak and broad excitation bands at ~346 and ~736 nm and a strong excitation band at ~502 nm. Five excitation bands at ~336, ~388, ~456, ~570, and ~682 nm with various intensities are observed for the emission band at 930 nm; these complicated excitation features are different from the excitation bands at ~354, ~400, and ~456 nm for the emission band at 1520 nm. The complicated features for excitation spectra at 930, 1160, 1260, and 1520 nm discussed above indicate that the newly generated Bi NIR centers at

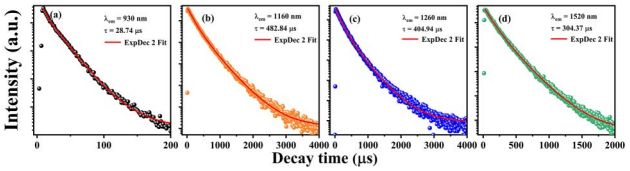

Fig. 4. Decay curves of (a) 930 nm, (b) 1160 nm, (c) 1260 nm, and (d) 1520 nm emission peaks of 11Al glass sample (λ_{ex} = 460 nm).

~930 and ~1520 nm are quite different from the NIR centers at ~1160 and ~1260 nm.

PL lifetime is another vital dynamic clue to illustrate the difference among the active Bi NIR centers. The decay curves of multiple active Bi NIR centers from 11Al glass sample are plotted in Figs. 4(a)–4(d). All the decay curves follow a double-exponential decay equation,

$$I(t) = A_1 \exp(-t/\tau_1) + A_2 \exp(-t/\tau_2), \quad (1)$$

where $I(t)$ is the intensity at time t; τ_1 and τ_2 are short and long decay components, respectively; and A_1 and A_2 are fitting constants. Fitting each curve to the equation produces τ_1 and τ_2, and the correlation coefficients always lie between 99.94% and 99.96%. The average fluorescence lifetimes $\bar{\tau}$ were calculated by the following formula:

$$\bar{\tau} = (A_1\tau_1^2 + A_2\tau_2^2)/(A_1\tau_1 + A_2\tau_2). \quad (2)$$

The obtained individual fluorescence lifetimes of 11Al glass sample at 930, 1160, 1260, and 1520 nm are 28.74, 482.84, 404.94, and 304.37 μs, respectively. Compared to that of Bi_5^{3+} (~5 μs)[32,33], Bi^+ (~460 μs)[30], and Bi^0 (~400 μs)[34], the great difference in fluorescence lifetime indicates that ~930 and ~1520 nm emission bands are truly rooted in other types of Bi species. Based on the results discussed above and previous study on the origin of Bi NIR centers, a reasonable conclusion can be drawn that the newly generated Bi NIR centers peaked at ~930 and ~1520 nm are formed by the interaction between interstitial Bi^0 and inherent defects generated by introducing AlN in germanate glass[35,36].

It is widely accepted that the valence states of Bi show hypersensitization to the variation of the glass local environment around them[22,37,38]. The details of the variation of the glass microstructure with the substitution of germanium by aluminum can contribute to the valence state change of Bi in the glasses. Hence, the local microstructure of the glass can help to extend our comprehension of the great enhancement and tunability of the Bi NIR emission. As shown in Fig. 5(a), the XRD patterns of xAl (x = 0–13) samples present no distinct diffraction peaks, confirming that the glass samples are in an amorphous state. In addition, the shape of the humps remains almost constant, which rules out the effect of nanocrystal formation on the Bi NIR emission with introduction of Al_2O_3.

To gain deep insight into the local microstructure feature of the glass, FTIR and Raman spectra of the glass samples are illustrated in Figs. 5(b) and 5(c), respectively. The strongest peak in

the Raman spectra located at 446 cm^{-1} is assigned to the symmetric stretching vibration of Ge–O–Ge in $[GeO_4]_6$ rings, while the latter peak lies at 524 cm^{-1} can be attributed to the symmetric breathing mode of Ge–O–Ge in $[GeO_4]_3$ or $[GeO_4]_4$ rings[39,40]. Although Al_2O_3 is introduced into the glasses, there is no significant shift of the Raman peaks, indicating that no transformation of $[GeO_4]_n$ (n = 3, 4, and 6) rings happens. Furthermore, two main absorption bands at 593 and 848 cm^{-1} and a wide absorption at 1036 cm^{-1} are observed in the FTIR spectra. The absorption band at 593 cm^{-1} is assigned to the symmetric stretching mode of Ge–O–Ge in the GeO_4 tetrahedra, and the absorption bands at 848 and 1036 cm^{-1} are due to the asymmetric stretching vibrations of Ge–O–Ge and the Ge–O stretching vibrations in the GeO_4 tetrahedra[41,42], respectively. Similarly, no distinct shift of the absorption bands is observed for the glass with various Al_2O_3, implying that the introduction of Al_2O_3 has little effect on the overall glass network.

To further probe the glass topology network, in particular of the short- to medium-range order of the glass samples with Al_2O_3 doping, the normalized ^{27}Al NMR spectra of glass samples are depicted in Fig. 5(d). There are three main types of aluminum coordination polyhedra, including octahedra (≈0 ppm), hexahedra (≈25 ppm), and tetrahedra (≈50 ppm) in the glass matrix[43,44]. As expected, a vast amount of the alumina in the glasses exits in tetrahedral (AlO_4) site, which acts as the network formerly in the glasses. To obtain visual conversion of the coordination polyhedra $[AlO_m]$ (m = 4, 5, and 6), Fig. 5(e) clearly presents the percentage of AlO_4, AlO_5, and AlO_6 in each glass sample. With the increase of Al_2O_3, the percentage of AlO_4 increased at the expense of AlO_5 and AlO_6 polyhedra. The variation of the NIR emission intensity almost coincides with that of AlO_4 species, indicating that the AlO_4 species play a vital role in affecting the multiple Bi NIR centers.

To the best of our knowledge, AlO_4 species usually act as network formers to connect the destroyed glass network, while $[AlO_5]$ and $[AlO_6]$ species commonly serve as network intermediates and modifiers, respectively. On one hand, the conversion from AlO_5 and AlO_6 species to AlO_4 species will strengthen the glass networks, thus triggering the chain reaction $Bi^{3+} \rightarrow Bi^{+} \rightarrow Bi^{0}$. Meanwhile, the interaction between Bi^0 and defects in the glass gets strengthened, which brings about the improvement of the newly generated emission bands at ~930 and ~1520 nm. On the other hand, the excessive AlO_4 bonding with the glass structure will form more Ge–O–Al bonds, resulting in local excess negative charges. In order to maintain charge balance, the low-valence Bi will be oxidized to a high-valence state, resulting in Bi^0 being oxidized as Bi^+ and Bi^{3+}, which exhibits the ultrabroadband tunable performance of Bi NIR emission and results in the decline of NIR emission intensity. To get deeper insight into this, the visible PL spectra from Bi^{3+} upon 350 nm excitation can be leveraged to verify it, as shown in Fig. 5(f). The intensity of the characteristic blue light emission from Bi^{3+} decreases monotonically upon the addition of Al_2O_3, and then an anomalous phenomenon occurs when the content of Al_2O_3 exceeding 11%, namely,

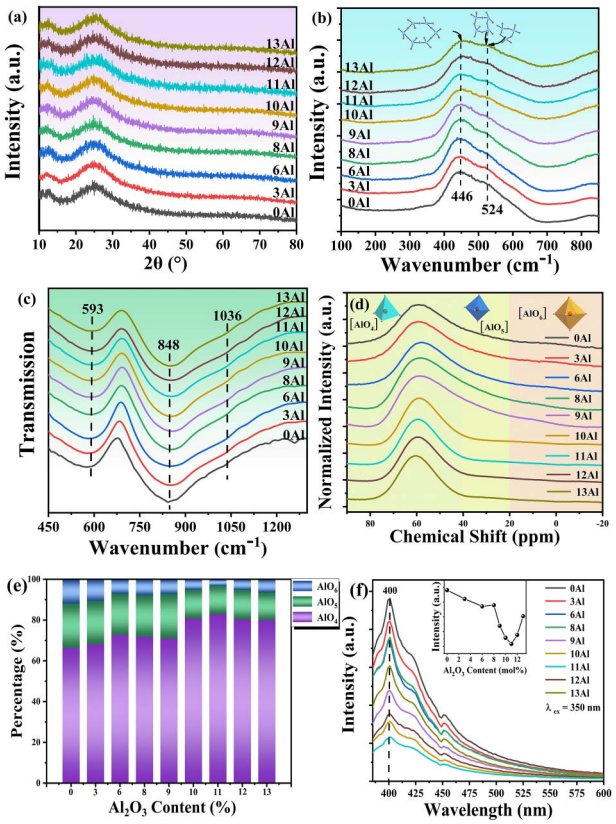

Fig. 5. (a) Normalized XRD spectra; (b) Raman spectra; (c) FTIR spectra; and (d) ^{27}Al 1D MAS NMR spectra (400 MHz) of the glass samples containing xAl_2O_3 (x = 0–13%), showing a gradual variation with increasing Al_2O_3 content, with the vertical scales (not shown) representing the intensity in arbitrary units, normalized to the maximum peak height in each spectrum; (e) percentage distribution of AlO_4, AlO_5, and AlO_6 by integrating area calculation of Gaussian multipeak fitting; the purple, green, and blue polyhedra beside the NMR spectra stand for Al tetrahedra, hexahedra, and octahedra, respectively. (f) Visible PL emission spectra (λ_{ex} = 350 nm) of Bi-doped nitridated germanate glasses containing xAl_2O_3 (x = 0–13%).

no red emission from Bi^{2+} is observed[45,46], which shows exactly the opposite trend in comparison with that of the NIR emission intensity. The results show clearly that the interaction between the two mechanisms discussed above contributes to the enhancement and ultrabroadband tunability of the multiple Bi NIR emissions, which predominantly depends on the concentration of Al_2O_3.

4. Conclusion

In conclusion, we successfully designed and fabricated a novel Bi–N co-doped germanate photonic glass, with highly efficient NIR emission (EQE of ~50%) and ultrabroadband tunable performance (850–1700 nm), via modulation of the short- to medium-range topological order of the glasses by regulating Al_2O_3 amounts. As revealed by optical and microstructure characterization, with the introduction of Al_2O_3, aluminum

tetrahedra AlO_4 increased at the expense of AlO_5 and AlO_6 polyhedra, which is favorable for the multiple Bi NIR emissions. Moreover, the parallel variation trend of bands at ~930, 1520, and ~1260 nm (Bi^0) implies that the newly generated NIR center is related to the Bi^0 center in the nitridated germanate glasses. Meanwhile, due to the replacement of Al_2O_3 with GeO_2, the formation of local excess negative charges promotes Bi^0 to be oxidized as Bi^+ and Bi^{3+}, which exhibits the ultrabroadband tunable performance of the multiple Bi NIR emissions. Importantly, this work opens an avenue for enhancing and regulating the multiple Bi NIR emissions and helps us to understand multiple Bi NIR emission behaviors in multicomponent glass, which shows great potential application in ultrabroadband wavelength-tunable glass fiber amplifier in optical communication.

Acknowledgement

This work was supported by the National Key R&D Program of China (No. 2021YFB2800500), the Research Program of Zhejiang Lab (No. 113014-AC2101), the National Natural Science Foundation of China (Nos. 51872095, U20A20211, and 62105297), and the Zhejiang Provincial Natural Science Foundation (Nos. LQ22A040011 and LZ23F050002).

References

1. J. Kaur, M. A. Khan, M. Iftikhar, M. Imran, and Q. E. U. Haq, "Machine learning techniques for 5G and beyond," IEEE Access **9**, 23472 (2021).
2. W. Wang, H. Wang, and G. Lin, "Ultrahigh-speed violet laser diode based free-space optical communication beyond 25 Gbit/s," Sci. Rep. **8**, 13142 (2018).
3. Y. Wang, L. Zhong, Z. Chen, D. Tan, Z. Fang, Y. Yang, S. Sun, L. Yang, and J. Qiu, "Photonic lattice-like waveguides in glass directly written by femtosecond laser for on-chip mode conversion," Chin. Opt. Lett. **20**, 031406 (2022).
4. S. Jetschke, S. Unger, A. Schwuchow, M. Leich, and J. Kirchhof, "Efficient Yb laser fibers with low photodarkening by optimization of the core composition," Opt. Express **16**, 15540 (2008).
5. A. B. Seddon, Z. Tang, D. Furniss, S. Sujecki, and T. M. Benson, "Progress in rare-earth-doped mid-infrared fiber lasers," Opt. Express **18**, 26704 (2010).
6. A. Herrera, F. Londoño, and N. Balzaretti, "Structural and optical properties of Nd^{3+} doped GeO_2-PbO glass modified by TiO_2 for applications in laser and fiber amplifier," Opt. Mater. **113**, 110884 (2021).
7. Q. Mao, B. Lan, and S. Zhou, "Crystallization control in Ni^{2+}-doped glass-ceramics for broadband near-infrared luminesce," J. Am. Ceram. Soc. **103**, 2569 (2020).
8. T. I. Yang, Y. C. Lin, S. C. Wang, and S. L. Huang, "Near-infrared broadband emission from glass-clad Cr-doped yttrium orthosilicate crystal fiber," Opt. Mater. Express **11**, 674 (2021).
9. K. Murata, Y. Fujimoto, T. Kanabe, H. Fujita, and M. Nakatsuka, "Bi-doped SiO_2 as a new laser material for an intense laser," Fusion Eng. Des. **44**, 437 (1999).
10. Y. Fujimoto and M. Nakatsuka, "Infrared luminescence from bismuth-doped silica glass," Jpn. J. Appl. Phys. **40**, L279 (2001).
11. Y. Ososkov, A. Khegai, S. Firstov, K. Riumkin, S. Alyshev, A. Kharakhordin, A. Lobanov, A. Guryanov, and M. Melkumov, "Pump-efficient flattop O+E-bands bismuth-doped fiber amplifier with 116 nm −3 dB gain bandwidth," Opt. Express **29**, 44138 (2021).
12. V. Dvoyrin, V. Mashinsky, L. Bulatov, I. Bufetov, A. Shubin, M. Melkumov, E. Kustov, E. Dianov, A. Umnikov, and V. Khopin, "Bismuth-doped-glass optical fibers—a new active medium for lasers and amplifiers," Opt. Lett. **31**, 2966 (2006).
13. S. V. Firstov, A. M. Khegai, A. V. Kharakhordin, S. V. Alyshev, E. G. Firstova, Y. J. Ososkov, M. A. Melkumov, L. D. Iskhakova, E. B. Evlampieva, and A. S. Lobanov, "Compact and efficient O-band bismuth-doped phosphosilicate fiber amplifier for fiber-optic communications," Sci. Rep. **10**, 11347 (2020).
14. Z. Zhang, J. Cao, J. Zheng, M. Peng, S. Xu, and Z. Yang, "Bismuth-doped germanate glass fiber fabricated by the rod-in-tube technique," Chin. Opt. Lett. **15**, 121601 (2017).
15. X. Li, M. Peng, J. Cao, Z. Yang, and S. Xu, "Distribution and stabilization of bismuth NIR centers in Bi-doped aluminosilicate laser glasses by managing glass network structure," J. Mater. Chem. C **6**, 7814 (2018).
16. F. Chen, Y. Wang, W. Chen, P. Xiong, B. Jiang, S. Zhou, Z. Ma, and M. Peng, "Regulating the Bi NIR luminescence behaviours in fluorine and nitrogen co-doped germanate glasses," Mater. Adv. **2**, 4743 (2021).
17. J. Cao, Y. Xue, J. Peng, X. Li, M. Huang, S. Xu, Z. Yang, and M. Peng, "Enhanced NIR photoemission from Bi-doped aluminoborate glasses via topological tailoring of glass structure," J. Am. Ceram. Soc. **102**, 1710 (2019).
18. R. Wan, Z. Song, Y. Li, Q. Liu, Y. Zhou, J. Qiu, Z. Yang, Z. Yin, Q. Wang, and D. Zhou, "Influence of alkali metal ions on thermal stability of Bi-activated NIR-emitting alkali-aluminoborosilicate glasses," Chin. Opt. Lett. **12**, 111601 (2014).
19. S. Khonthon, S. Morimoto, Y. Arai, and Y. Ohishi, "Redox equilibrium and NIR luminescence of Bi_2O_3-containing glasses," Opt. Mater. **31**, 1262 (2009).
20. B. Xu, S. Zhou, M. Guan, D. Tan, Y. Teng, J. Zhou, Z. Ma, Z. Hong, and J. Qiu, "Unusual luminescence quenching and reviving behavior of Bi-doped germanate glasses," Opt. Express **19**, 23436 (2011).
21. V. G. Truong, L. Bigot, A. Lerouge, M. Douay, and I. Razdobreev, "Study of thermal stability and luminescence quenching properties of bismuth-doped silicate glasses for fiber laser applications," Appl. Phys. Lett. **92**, 041908 (2008).
22. L. Wang, J. Cao, Y. Lu, X. Li, S. Xu, Q. Zhang, Z. Yang, and M. Peng, "*In situ* instant generation of an ultrabroadband near-infrared emission center in bismuth-doped borosilicate glasses via a femtosecond laser," Photonics Res. **7**, 300 (2019).
23. X. Li, F. Hu, M. Peng, and Q. Zhang, "Crystallization kinetics and enhanced Bi NIR luminescence of transparent silicate glass-ceramics containing Sr_2YbF_7 nanocrystals," J. Am. Ceram. Soc. **100**, 574 (2017).
24. W. Wang, J. Yuan, D. Chen, Q. Qian, and Q. Zhang, "Enhanced broadband 1.8 μm emission in Bi/Tm^{3+} co-doped fluorogermanate glasses," Opt. Mater. Express **5**, 1250 (2015).
25. J. Xiao, J. Cao, Y. Wang, X. Li, X. Wang, J. Zhang, and M. Peng, "Temperature dependent energy transfer in Bi/Er codoped barium gallogermanate glasses for tunable and broadband NIR emission," J. Mater. Chem. C **7**, 10544 (2019).
26. M. Peng, C. Zollfrank, and L. Wondraczek, "Origin of broad NIR photoluminescence in bismuthate glass and Bi-doped glasses at room temperature," J. Phys. Condens. Matter **21**, 285106 (2009).
27. N. Zhang, J. Qiu, G. Dong, Z. Yang, Q. Zhang, and M. Peng, "Broadband tunable near-infrared emission of Bi-doped composite germanosilicate glasses," J. Mater. Chem. **22**, 3154 (2012).
28. B. Xu, S. Zhou, D. Tan, Z. Hong, J. Hao, and J. Qiu, "Multifunctional tunable ultra-broadband visible and near-infrared luminescence from bismuth-doped germanate glasses," J. Appl. Phys. **113**, 083503 (2013).
29. J. Cao, L. Wondraczek, Y. Wang, L. Wang, J. Li, S. Xu, and M. Peng, "Ultrabroadband near-infrared photoemission from bismuth-centers in nitridated oxide glasses and optical fiber," ACS Photonics **5**, 4393 (2018).
30. J. Cao, S. Xu, Q. Zhang, Z. Yang, and M. Peng, "Ultrabroad photoemission from an amorphous solid by topochemical reduction," Adv. Opt. Mater. **6**, 1801059 (2018).
31. J. Cao, A. Reupert, Y. Ding, and L. Wondraczek, "Intense broadband photoemission from Bi-doped ZrO_2 embedded in vitreous aluminoborate via direct melt-quenching," J. Am. Ceram. Soc. **105**, 2616 (2022).
32. R. Cao, M. Peng, J. Zheng, J. Qiu, and Q. Zhang, "Superbroad near to mid infrared luminescence from closo-deltahedral Bi_5^{3+} cluster in $Bi_5(GaCl_4)^3$," Opt. Express **20**, 18505 (2012).
33. A. N. Romanov, Z. T. Fattakhova, A. A. Veber, O. V. Usovich, E. V. Haula, V. N. Korchak, V. B. Tsvetkov, L. A. Trusov, P. E. Kazin, and V. B. Sulimov, "On the origin of near-IR luminescence in Bi-doped materials. (II). Subvalent

monocation Bi^{+} and cluster Bi_5^{3+} luminescence in $AlCl_3/ZnC_{l2}/BiCl_3$ chloride glass," Opt. Express **20**, 7212 (2012).
34. M. Peng, B. Sprenger, M. A. Schmidt, H. Schwefel, and L. Wondraczek, "Broadband NIR photoluminescence from Bi-doped $Ba_2P_2O_7$ crystals: insights into the nature of NIR-emitting bismuth centers," Opt. Express **18**, 12852 (2010).
35. V. Sokolov, V. Plotnichenko, and E. Dianov, "Origin of near-IR luminescence in Bi_2O_3–GeO_2 and Bi_2O_3–SiO_2 glasses: first-principle study," Opt. Mater. Express **5**, 163 (2015).
36. Q. Chen, W. Jing, Y.-Y. Yeung, M. Yin, and C.-K. Duan, "Mechanisms of bismuth-activated near-infrared photoluminescence–a first-principles study on the $MXCl_3$ series," Phys. Chem. Chem. Phys. **23**, 17420 (2021).
37. Y. Zhao, L. Wondraczek, A. Mermet, M. Peng, Q. Zhang, and J. Qiu, "Homogeneity of bismuth-distribution in bismuth-doped alkali germanate laser glasses towards superbroad fiber amplifiers," Opt. Express **23**, 12423 (2015).
38. H. Masai, T. Suzuki, and Y. Ohishi, "Relationship between near-infrared emission of bi-doped glass and preparation conditions," Sens. Mater. **30**, 1533 (2018).
39. H. Verweij and J. Buster, "The structure of lithium, sodium and potassium germanate glasses, studied by Raman scattering," J. Non-Cryst. Solids **34**, 81 (1979).
40. J. Alvarado-Rivera, D. A. Rodríguez-Carvajal, M. C. Acosta-Enríquez, M. B. Manzanares-Martínez, E. Álvarez, R. Lozada-Morales, G. C. Díaz, A. de Leon, and M. E. Zayas, "Effect of CeO_2 on the glass structure of sodium germanate glasses," J. Am. Ceram. Soc. **97**, 3494 (2014).
41. P. Pascuta and E. Culea, "FTIR spectroscopic study of some bismuth germanate glasses containing gadolinium ions," Mater. Lett. **62**, 4127 (2008).
42. E. Culea, L. Pop, M. Bosca, T. Rusu, P. Pascuta, and S. Rada, "FTIR spectroscopic study of some lead germanate glasses," J. Phys. Conf. Ser. **182**, 012061 (2009).
43. P. F. McMillan, W. T. Petuskey, B. Coté, D. Massiot, C. Landron, and J.-P. Coutures, "A structural investigation of CaO-Al_2O_3 glasses via ^{27}Al MAS-NMR," J. Non-Cryst. Solids **195**, 261 (1996).
44. D. R. Neuville, L. Cormier, and D. Massiot, "Al coordination and speciation in calcium aluminosilicate glasses: effects of composition determined by ^{27}Al MQ-MAS NMR and Raman spectroscopy," Chem. Geol. **229**, 173 (2006).
45. X. Liu, C. Cheng, X. Li, Q. Jiao, and S. Dai, "Controllable ultra-broadband visible and near-infrared photoemissions in Bi-doped germanium-borate glasses," J. Am. Ceram. Soc. **103**, 183 (2020).
46. Q. Dong, P. Xiong, J. Yang, Y. Fu, W. Chen, F. Yang, Z. Ma, and M. Peng, "Bismuth activated blue phosphor with high absorption efficiency for white LEDs," J. Alloys Compd. **885**, 160960 (2021).